Chapter 8

Magnetoencephalography (MEG)

Andreas A. Ioannides

Abstract

Magnetoencephalography (MEG) encompasses a family of non-contact, non-invasive techniques for detecting the magnetic field generated by the electrical activity of the brain, for analyzing this MEG signal and for using the results to study brain function. The overall purpose of MEG is to extract estimates of the spatiotemporal patterns of electrical activity in the brain from the measured magnetic field outside the head. The electrical activity in the brain is a manifestation of collective neuronal activity and, to a large extent, the currency of brain function. The estimates of brain activity derived from MEG can therefore be used to study mechanisms and processes that support normal brain function in humans and help us understand why, when and how they fail.

Key words: Bioelectromagnetic forward and inverse problem, superconductivity, equivalent current dipole (ECD), magnetic field tomography (MFT).

1. Introduction

Brain function is founded on electrical activity within and between *neurons*. The activity of individual neurons is too small to be detected with sensors placed outside the head. The activity of neurons within circumscribed brain areas a few millimeters to a centimeter across is sufficiently differentiated from the activity of other neurons to justify thinking of these areas as segregated islands of processing. The processing within and interactions between these areas relies again on electrical activity, albeit, now it reflects not only neuron-to-neuron exchanges, but also collective action, coherent in time, from a large population of neurons that probably share similar properties (e.g. selectivity to some stimulus feature). This collective excitation of local network electrical activity in the brain is large enough to produce measurable changes

Fahmeed Hyder (ed.), *Dynamic Brain Imaging: Multi-Modal Methods and In Vivo Applications, vol. 489*

DOI 10.1007/978-1-59745-543-5 Springerprotocols.com

in both the electrical potential on the surface of the head, the electroencephalogram (EEG) and the magnetic field a few centimeters beyond, the magnetoencephalogram (MEG), which is the subject of this narrative.

MEG was introduced some 40 years ago *(1)* but stayed for much of the time within small academic groups mainly in physics departments, as a novelty area between physics and biology. Although what was needed for the technology to become clinically relevant was correctly identified early on *(2)*, the field reacted rather slowly because the requirements were beyond what academic departments or small companies could afford. Two other reasons delayed the emergence of MEG into modern neuroimaging. First, the signal of an MEG channel after the usual processing and averaging looks just like an EEG signal, so many saw MEG as an expensive EEG technology. Some still do so today. Second, it was known for well over a century that the mathematical problem of recovering the generators from the MEG and/or EEG signal has no unique solution *(3)*. The non-uniqueness of the bioelectromagnetic inverse problem is an undeniable theoretical fact, but a rather benign problem in practice. Evidence that real-time information about brain function was available from MEG at not only excellent temporal resolution but also at fine spatial detail became available in the 90s from novel analysis of multichannel MEG data *(4,5)*. Eventually, helmet-like systems allowed the mapping of the instantaneous magnetic field all around the head in an instance. The analysis of the resulting signals provided, for the first time, a view of dynamics of brain function across the entire brain *(4)*.

From the numerous reviews of MEG, the 1993 work from the Helsinki group remains the most comprehensive and informative *(6)*. More recent reviews have emphasized how, despite the issues regarding the inverse problem, putative sources can be estimated *(7)* and, increasingly more often, how beam forming techniques can usefully scan the source space point by point *(8)*. Most of the techniques discussed in the literature use linear methods for extracting estimates for the generators. Heuristic analysis *(9)* and theory *(10)* suggest that a specific form of non-linearity is necessary for the solutions to possess expected properties for localized distributed sources. Dealing successfully with the computational penalty that goes with non-linearity, leads to reliable tomographic estimates of brain activity from instantaneous MEG signals. Magnetic Field Tomography (MFT) is the name given to the resulting method of extracting estimates of brain activity *(11)*. MFT solutions can scrutinize brain function at multiple spatiotemporal scales. In the spatial domain, the range covers details a few millimeters across (distinguishing activity within individual cytoarchitectonic areas) to mapping across almost the entire brain. In the time domain, events can be analyzed at timescales from a fraction

of a millisecond to minutes and hours *(12)*. It thus becomes possible to extract from the same set of MEG data views of local and global activity and patterns of connectivity in this wide spatiotemporal scales of bewildering complexity *(13)*.

Here, we provide an overview of MEG, covering basic principles, measurements, source reconstruction, and finally examples to demonstrate the different types of output that can be extracted from the analysis of MEG recordings and by implication what is the relevance of such output to neuroscience. The next section, *Materials*, first describes in simple terms possible neural mechanism that may be responsible for coherent electrical activity from many neurons. It then outlines how the well-understood laws of electromagnetism and properties of the head explain the generation of, and differences between the EEG and MEG signals. Finally, this section outlines the instruments that allow the detection of the MEG signal outside the head. The *Forward and Inverse Problems* section outlines how one can compute the signal generated by a given configuration of generators (the forward problem) and how one can derive estimates for the generators from the measurements (inverse problem). The next section, *Output of MEG*, provides a flavor of the output of MEG analysis with emphasis on aspects that are unique to this technology. We finish with *Notes* where the advantages and disadvantages of MEG are discussed.

2. Materials

This section first outlines the likely neuronal mechanisms responsible for the generation of the MEG and EEG signal and then describes the basic elements of the hardware used for the detection of the MEG signal.

2.1. Neural Mechanisms

The smallest detectable MEG signal requires concerted action from many neurons numbering at a minimum many hundreds. These neurons must be arranged in a similar way in space and they must be activated in near synchrony. The very presence of a good size MEG and EEG signal is evidence for dual organization of neurons: a spatial organization in the way they are grouped together in space and large scale synchrony in the way their activity is organized in time. It is generally believed that relatively slow changes in electrical activity associated with post-synaptic potentials (PSP) at the apical dendrites of large pyramidal neurons are the main contributors to the MEG signal. Large pyramidal neurons are prime candidate generators of MEG signals because their elongated shape is ideal for producing strong primary currents. Furthermore they are arranged in parallel in the cortex so the

net impressed current from nearby large pyramidal neurons will tend to sum up constructively. It is very likely that a large part of the MEG signal is indeed due to slow PSPs in the apical dendrites of pyramidal neurons, especially at frequencies well below 100 Hz. For this standard mechanism, typical estimates require about a million synapses to be simultaneously active to produce a measurable MEG signal *(6)*. MEG activity at frequencies well above 100 Hz is likely to be produced by synchronous action potentials *(14)*.

2.2. Recording the MEG Signal and Isolating the Contribution from the Brain

Although the MEG signal is generated by the collective activity of a large number of neurons, its strength is extremely weak compared to typical terrestrial magnetic fields. The earth's magnetic field is about a billion times as strong, while the usual urban environment at frequency ranges that overlap the ones of interest in MEG is still many orders of magnitude higher than the strongest MEG signal from a normal human brain. A pre-requisite for useful MEG measurements is therefore the availability of sensors that can detect the weak magnetic fields generated by the brain. Also required are methods that can exclude the large ambient fields and tools that can separate out the signal of interest from any remaining interfering signals from the environment and other signals generated by the body of the subject that are often considerably stronger than the signal of interest.

The basic MEG measurement relies on the detection of the electrical current in a small loop of wire, typically about one centimeter across, induced by the change in the magnetic field component perpendicular to the loop surface. Measurement of the induced current determines the value of the change in the magnetic field. Usually a set of coils is arranged as a gradiometer to emphasize nearby signals from the brain at the expense of distant sources. The detection of the minute magnetic field changes outside the head generated by electrical currents in the brain is measured by coupling the coil or gradiometer to an extremely sensitive "superconducting quantum interference device" (SQUID). SQUIDS, as the name implies, rely for their exquisite sensitivity on superconductivity and together with their sensing coils must be kept at extremely low temperatures, just a few degrees above absolute zero. To achieve this, sensing coils and SQUIDS are kept in a thermos-like container, the Dewar, which under normal operating conditions is filled with liquid helium. In modern systems, the bottom of the Dewar is shaped into a helmet with well over one hundred, nowadays a few hundred, sensing coils evenly distributed on its inner surface. Just a few millimeters away, on the other side of the insulating layer, at normal room temperature, a subject can safely place his/her head inside the helmet. Each sensing coil samples the local magnetic field and the full set of sensing coils can be "scanned" a few thousand times

a second. Each scan delivers an independent measurement of the instantaneous magnetic field just outside the head. Although SQUID technology is now mature providing turn-key systems for whole-head MEG devices, its basic cryogenic requirements make it very expensive. In recent years, atomic magnetometry, a method of measuring magnetic fields based on the interaction of resonant light with atomic vapor, has emerged as a potentially cheaper alternative to SQUID based sensors *(15)*.

The second requirement, separating the signal of interest from the larger ambient background and other interfering signals, is achieved by a combination of passive shielding, use of gradiometer design either in hardware for the sensing coils coupled to the SQUIDS or in software using additional reference channels. Other signal processing techniques, e.g. Independent Component Analysis (ICA) *(16)* coupled to the use of information from auxiliary channels like the electrooculogram (EOG) and electrocardiogram (ECG) can effectively eliminate biological and other artifacts. The combination of the exquisite SQUID sensitivity with these hardware and software methods allows the measurement of the magnetic field generated by the brain with little contamination.

In a modern MEG system, typically a few hundred sensing coils, each coupled to its own SQUID, are housed at the bottom of the helmet-shaped Dewar, distributed so that they capture evenly the magnetic field just outside the head. The magnetic field for just one "timeslice" can be mapped by recording the signal from each sensor independently from, and for all practical purposes simultaneously with, the signal of each other sensor. In one second, a few thousand such timeslices can be recorded so that successive timeslices provide a movie of the instantaneous change in the magnetic field just outside the head. Since, as we will shortly describe, the speed of propagation from the generators to the sensors is the speed of light, the MEG signal change corresponds to the instantaneous change of the electrical current density in the brain generated by neuronal activity. The peaks of the signal generated by the brain are about two orders of magnitude higher than the device noise level, so the map of the magnetic field not only has exquisite time resolution (a fraction of a millisecond) but is also a very clean map of the topography of the magnetic field just outside the head.

3. Forward and Inverse Problem

The determination of the EEG and MEG signal from the knowledge of the sources, the electrical properties of their biological environment and the configuration of the measuring devices

is known as the forward problem. The estimation of generator strength, location and timecourse from the EEG and MEG signal and the knowledge of electrical properties of their biological environment and the configuration of the measuring devices is known as the inverse problem. The laws of electromagnetism define what can be asked of the data and how the forward and inverse problems should be tackled, in particular what a priori assumptions can be made about the generators. The forward and inverse problem will be considered, describing in each case the theoretical framework established by the laws of electromagnetism and its implications for useful MEG (and sometimes EEG) applications

3.1. The Forward Problem

It is useful to separate the full current density into two terms. In general, we are interested in the first term known as impressed currents because they describe the active currents generated by energy-demanding neuronal activity. The remaining currents make up the second term; they describe the passive currents that flow as a result of the impressed currents in the biological medium. Impressed currents of an individual neuron cannot be directly detected by either MEG or EEG because they are too weak. Even under the most favorable conditions, a detectable signal can only be generated by the collective activity of at least many hundreds of neurons spread over 1 mm^2 or larger cortical patches. At this spatial scale, the appropriate terms that best separate the full current density into active and passive elements are referred to as primary current density and volume or return currents respectively. The primary current density depends on both intracellular currents and the local extracellular currents. The intracellular currents are closely related to the local impressed currents. Since these ionic flows are along axons and dendrites, the net contribution from a single neuron is a sum of vectors each pointing along the long axis of the corresponding active dendrite or axon. The overall primary current density generated by intracellular currents is the vector sum of contributions from active neurons, which is therefore strongly dependent on the overall arrangement of neurons. The flow of extracellular currents along the local conductivity gradients is determined mainly by cell membranes. For each focal neuronal activity, the local arrangement of cells determines the combined effect of both intracellular and extracellular currents and therefore shapes the resulting primary current density. The source space is a convenient label for the region of space where the primary current density can be non-zero, and it includes the entire brain. Primary currents can be thought of as the generators of the volume or return currents, i.e., the large-scale passive electrical current flowing in the "volume conductor", in the brain at large and bounded by the highly resistive skull. These large-scale passive electrical currents do not contribute to the magnetic field, except where they "twist" at boundaries with

sharp changes in conductivity, especially the skull. In the special case that only concentric spherical boundaries of changes in conductivity are present, the magnetic field generated outside a conductor is given by an analytical expression *(17)*. Furthermore, the laws of electromagnetism and spherical symmetry define explicitly which generators can produce an external magnetic field and which are magnetically silent, i.e. they do not produce an external magnetic field no matter how strong they are. Specifically, radial components of the current density are magnetically silent sources. The magnetic field generated by tangential components of the current density can be written analytically in a form that depends on the center of the conducting sphere(s) and it does not depend on either the conductivities of the different compartments or the radii of the concentric shell(s), as long as the magnetic field is computed outside the conductor (last spherical shell). Finally, for a spherical conductor, the radial magnetic field, i.e. the component of the magnetic field (outside the head) pointing away from the center of the conducting sphere depends only on the primary currents. The magnetic field for realistic head shapes can be computed accurately and fast using a set of overlapping spheres appropriately chosen for each sensor *(18)*. The skull is smooth and nearly spherical; so, the convenient and relatively simple spherical model can provide an excellent estimate for the second term, except around openings like the eye sockets or parts of the skull that deviate substantially from the spherical model.

The EEG forward problem poses real difficulties in practice. The accurate computation of EEG signal is more demanding because it depends strongly on details of the conductivity profile. The differences in the forward problem for MEG and EEG signals have two main consequences. First, the relationship between neuronal activity is easier to model for MEG. On the one hand, the skull is transparent to magnetic fields and highly resistive to electrical currents (that must cross it to produce the scalp EEG) and, on the other, the effect of the conducting medium can be approximated by simple models for accurate computations of the magnetic field but have to be described in detail for the computation of the surface potential. Second, the EEG is influenced strongly by both radial and tangential electric currents while MEG is only sensitive to tangential ones.

The laws of electromagnetism endow both EEG and MEG signals with a direct relationship with the neuronal sources. Specifically, the electric and magnetic fields propagate from the (neuronal source) generator site with the speed of light. Since the sensors are just some centimeters away, for all practical purposes, the effect is immediate: a change in the source electrical activity in the brain produces an immediate change in the MEG and EEG signal. This is in sharp contrast with other neuroimaging methods like positron emission tomography (PET) and functional

magnetic resonance imaging (fMRI) that rely on changes in blood flow or content (e.g. radioactive labeling or oxygenation) and therefore produce indirect correlates of neuronal activity with delays that are, at best, a good fraction of a second in the case of fMRI and minutes in the case of PET.

Finally, the forward problem is linear as a direct consequence of the linearity of the laws of electromagnetism. In other words, the electric and magnetic field generated by any combination of instantaneous current elements is simply the sum of individual contributions from each element. In the case of continuous primary current density, the instantaneous electric and magnetic field can be computed by integrating the contributions from each small volume element in the source space. In the case of a spherical model, the source space for MEG includes only regions where neurons and possibly white matter exists, any intervening regions and boundaries are not part of the source space as long as they do not generate primary currents.

3.2. Inverse Problem

In contrast to the forward problem, the inverse problem has no unique solution, a mathematical fact that was already demonstrated over 150 years ago *(3)*. Simply stated, it is impossible to reconstruct uniquely the electrical current density inside the head from MEG and/or EEG measurements. Even if we knew exactly the electrical potential on the surface of the head and the magnetic field everywhere outside the head, we would still be unable to determine the currents inside the head. In practice, non-uniqueness is much less of a problem than would appear from the dry mathematical statements. By definition, silent sources cannot be recovered and noise and sparse sensor coverage further limit what can be reliably extracted about the non-silent part of the current density vector. Nevertheless, what is often required of the data is to provide reliable estimates about which areas of the brain were preferentially activated by some stimuli or tasks and when. This limited objective is often satisfied with estimates of the timecourse of the non-silent part of the source configuration. The key question in practice is how accurately and reliably one can recover the non-silent part of the primary current density.

A unique solution of the biomagnetic inverse problem can be obtained by introducing constraints for the form of the generators. Two types of constraints are particularly popular *(6)*. The first assumes that the generators are one or more point-like sources, or current dipoles. Dipole source localization solutions are often interpreted as representatives for their neighborhood and are referred to as equivalent current dipoles (ECD). The second family of popular source localization methods assumes that the continuous current density can be written as a linear sum of (weighted) functions, each defining the sensitivity profile or lead fields for one of the sensors. These methods, known as minimum

norm (MN) or weighted minimum norm (wMN) solutions, are popular because they lead to a linear system of equations which allows standard pseudoinverse techniques to define the inverse operator that can then be applied directly to the data. Theoretical scrutiny of the mathematical foundation of the inverse problem shows that neither current dipoles nor linear solutions are adequate. Minimum norm is not appropriate for tomographic localization for a rather subtle reason; although the forward problem is linear, the optimal algorithm for tackling the inverse problem cannot be linear *(10)*. The laws of electromagnetism provide no justification for expressing the full primary current density vector as a (weighted) sum of lead fields. Physics allows only the direction of the primary current density to be so represented, but this leads inevitably to a non-linear relationship between the measurements and the distribution of generators. This conclusion was reached first on the basis of simulation studies leading to the standard form of magnetic field tomography (MFT) *(9)*. In summary, the basic assumption of MFT is that a (weighted) linear expansion in terms of lead fields can represent only the *direction* of the current density. This is as much as can be deduced from the underlying physics for fixed detectors and conductivity profile. The strength of the current density must be determined more explicitly from the MEG signal itself. Specifically, the full current density must be obtained from a highly non-linear system of equations for each snapshot of data. It is precisely because linearity is lost, that a direct appeal to the data must be made on every timeslice of the data and a new non-linear system of equations must be solved each time. In this sense, MFT draws on all available information in the MEG signal. The advantage of the form of non-linearity introduced by MFT is the ability to recover activity that can be either spatially sharp or distributed, thus leading to tomographic description of the generators with practically no a priori assumptions. However, non-linearity comes with a heavy computational cost, but a rather affordable penalty today, thanks to modern computers.

To appreciate the subtle difference between various inverse problem approaches, it is necessary to consider in detail how the lead fields can be used to construct estimates of the unknown current density vector. The similar nature of different linear methods, e.g. of MN and wMN and LORETTA *(19)*, and how they differ from other non-linear methods like MFT and FOCUSS *(20)* can be best demonstrated by expressing the unknown current density as a series expansion of lead fields with different orders in the series modulated by the modulus of the current density raised to some power, as described in detail elsewhere *(10, 21)* and in outline in Appendix 1.

In the early 1990s, numerous comparisons between MFT and ECD models with computer generated data *(9)*, MEG

signals evoked by stimuli *(22)* and epileptic activity *(23)*, all demonstrated the ability of MFT to identify distinct foci of activity as their strength changed while ECD models described them as wandering dipoles through the brain. In the last ten years, accurate MFT reconstructions have been demonstrated with many applications and with the emphasis recently placed on reconstructions of real-time data, i.e. for single timeslices of single trials *(4, 14)*.

4. Output of MEG

Neuroscience has, at its disposal, a plethora of exquisite techniques to study neural activity. In the vast majority of cases, the output of techniques is sufficiently constrained to limit the choices of the researcher to qualitatively one distinct category of output. The researcher has to perfect the technique to obtain the data of the highest possible quality, but she/he cannot change the qualitative nature of the neural events she/he is studying. For example, in a microstimulation experiment, one may worry about how large an area is excited but, one is certain that what is examined is the disruptive effect of injecting a current that perturbs the local neural interactions. Similarly, when one uses fMRI or PET, one can safely assume that one measures correlates of neural function mediated by blood supply and, hence, over delays of seconds. With MEG, the case is somewhat different because the method allows one to focus either at fine detail in space and time, and/or within a small area, or across the brain at timescales ranging from a fraction of a millisecond to hours. Quantitative changes in the choice of what spatiotemporal scales to consider imply sensitivity to qualitatively different neuronal events and organization. Using MFT, for example, to image in real time, one can follow changes in the brain at a fraction of a millisecond *(14)*, i.e. at a temporal resolution that is about one order of magnitude *higher* than the characteristic scale that it takes one brain area to influence another (this also demands working close to the noise level of the measurements). A safer but less ambitious approach, and still rather rare in the field, would study tomographically brain activity extracted from real time (un-averaged) MEG data filtered in the range say 3–200 Hz and after removing the interference from the mains and its harmonics and contributions from strong physiological sources like the eyes and heart. Such analysis would then map brain activity at about the timescale of transitions in the brain. The output of real-time tomographic analysis is an attempt to describe what is happening in the brain with minimal assumptions. Assuming that such a reconstruction is possible, statistics on the tomographic solutions

can then be performed just as is done for fMRI data, but with far richer access to neuronal dynamics *(12, 13)*. The popular ECD method of analysis, using point-like models for the generators, will not work with real time MEG signals because rarely, if ever, the activity of the normal brain is dominated by a single focal source. Early MEG experiments with one or only a few sensors could only obtain signal topographies by repeating a task or delivering the same stimulus many times while recording the resulting MEG signal. Although this is no longer necessary with multi-channel systems, averaging remains a simple and powerful way of drastically reducing the complexity of the data. Averaging emphasizes activity that is precisely time-locked to an external stimulus which is more likely to be dominated by contributions that are fairly focal. As a result, ECD analysis often provides a very good fit for the average evoked response. Some of the apparently good fits obtained by ECD modeling of average data do reflect the true nature of the generators. However, the average makes up only a tiny part of the single trial MEG signal. Even the actual average MEG signal is often a collection of distinct responses that do not belong together *(5, 24)* and the apparent success of the ECD model could be a mirage with some of the real generators a fair distance away from the ECD loci *(25, 26)*. The likelihood always remains that a very large part of the activity related to the processing of the stimulus remains unexplained, lost in the process of averaging before any analysis is made, as recent studies have shown *(27, 28)*, but see reference *(29)* for a different view.

Despite the huge potential of MEG, its usefulness has been questioned. MFT has been for many years the only technique capable of real-time tomographic reconstructions, initially because its implementation demanded what, at the time, was super-computing resources *(30)*. What single trial MFT solutions described (tomographic estimates of real-time brain activity) was often confused with descriptive measures of power of the MEG signal and ECD fits to average data. Tapping into single trial data tomographically was giving a view of brain activity that was far more dynamic than the smooth evolution produced by fits to average data using ECDs that the MEG and EEG communities were familiar with for decades. Although this dynamic view was much more in step with invasive measures of activity, it was not adopted initially because the experience from ECD analysis and the non-uniqueness of the inverse problem had convinced many practitioners that tomographic analysis was impossible. In recent years, other techniques have emerged making better use of the information in the raw MEG signal than the averaging. Results obtained with these methods have vindicated many of the early MFT results. Beamformer techniques, in particular, have been increasingly used recently with good effect *(8)*. One of the most exciting results of MFT analysis was the identification of

V1 modulation well within 100 ms by activity in the amygdala some 40–50 ms earlier *(4, 31, 32)*. This early amygdala and V1 activations and their interaction were identified in the responses elicited by emotional faces, providing support for the existence of a low route to the amygdala as postulated by Le Doux *(33)*. In addition to the obvious theoretical importance of this observation for normal brain function, it was also found that early and late amygdala and V1 activations, and the interaction of these and other areas (fusiform gyrus and inferior frontal cortex) were different in normal subjects and schizophrenics *(31, 32, 34)*. These MFT findings were recently reproduced with remarkable consistency in the timing of amygdala and V1 activity as an event-related synchronization in response to fearful faces using beamformer techniques *(35)*.

We conclude this section with examples demonstrating how the nature of the output changes as we move from MEG signals to tomographic estimates of activity, and measures that describe the properties of groups of trials. We will show examples that progress systematically in complexity using either single trial data or the average of a small number of trials to mine the MEG data. The first example, **Fig. 8.1**, shows how strong features can be extracted directly from a signal signature, almost a direct reading of the MEG single trial signals. The data were collected from a median nerve stimulation that was strong enough to elicit a finger twitch. The first 11 responses are shown by the triggers collected simultaneously with the MEG signal (**Fig. 8.1a**). This unusually strong stimulus and the superficial location of the primary somatosensory cortex (S1) make the first cortical responses elicited by each stimulation almost visible in the raw signal. A virtual sensor can be constructed in this case (see below) which enhances the pattern of signal produced by S1 while reducing other signals. Despite this enhancement, the actual evoked response is barely discernible in the presence of other similar activations (**Fig. 8.1b**). The evoked response becomes easier to see in the zoomed version covering the third and fourth median nerve stimulations (**Fig. 8.1c**). In this figurine, two more properties of the MEG signal are evident. First, the evoked response is similar from trial-to-trial in its slow envelope but the fast transients riding on it are highly variable from trial to trial. Second, the virtual sensor (VS) output for the signal from the brain is always much higher than the system noise, a direct demonstration of the high dynamic range of MEG. The VS for the system noise is the barely distinguishable trace hugging the zero level horizontal axis; it is obtained by processing the MEG signal recorded when no subject is in the shielded room in exactly the same way as the signal from the subject. The VS is constructed by taking the difference of the means of the 7 strongest positive and 7 strongest negative MEG channels

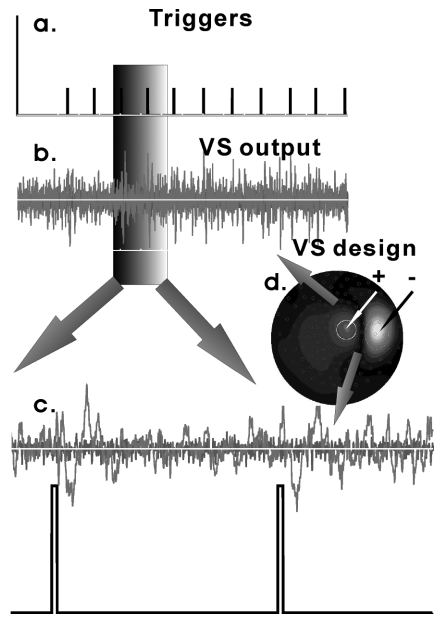

Fig. 8.1. Virtual sensor output for a strong signal. (**a**) The delivery of a median nerve stimulation is marked by a trigger and collected together with the MEG signal. (**b**) The MEG signal for the real measurement as marked by the triggers in (**a**) and for a recording of the noise level of the system (no subject in the MEG room). (**c**) A zoomed version of the VS output (*top*) and corresponding third and fourth triggers. (**d**) The VS is computed from the difference of means of the 7 most positive and 7 most negative MEG sensors. (*See* Color Plate)

(**Fig. 8.1d**). Weaker stimuli, e.g. typical visual stimuli, or median nerve stimulation below motor threshold, produce responses that are not easily discernible from the background activity.

The second example (**Fig. 8.2**) shows the reliable extraction of the expected (but relatively weak) activity through single trial tomographic (MFT) analysis using only a small number *(6)* of trials. **Figure 8.2a** shows single trial activations (purple and red curves) for left visual cortex and fusiform gyrus (FG) elicited by face and checkerboard stimuli presented in the lower right part of the visual field. The left and right columns show results for activation curves from the left dorsal V1 and FG respectively. The different rows show the responses when the presentation of the stimuli and the subject's attention is on one or other category of stimuli. It is critical to realize that these activation curves are extracted from tomographic solutions for each timeslice and single trial and they are much more specific than any signal or virtual sensor for that matter. Since the solutions are obtained independently for each timeslice and trial, simple but powerful estimates of the signal power (SP) and noise power (NP) and hence their ratio, signal to noise power (SNR) can be obtained from the activation curves of only six trials using 20 ms sliding windows across the

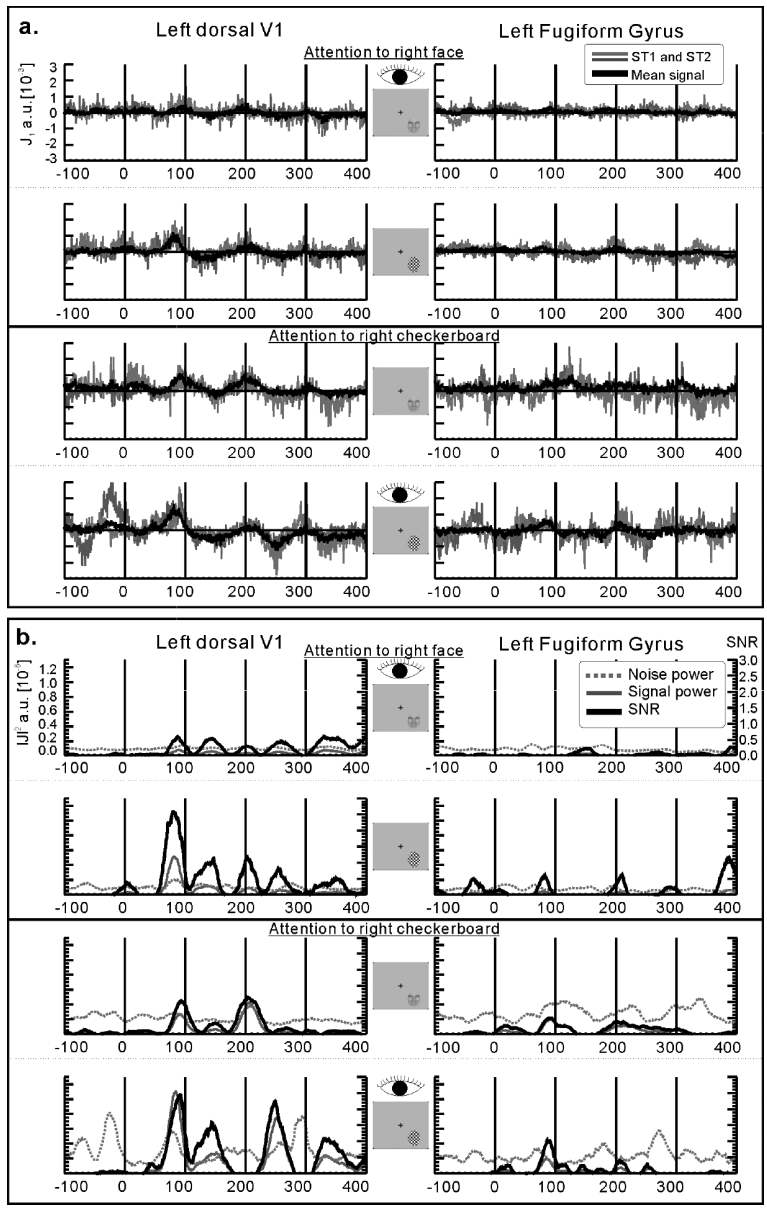

Fig. 8.2. (**a**) Two single trial activation curves extracted from tomographic MFT solutions with region of interest in the left dorsal V1 and the Left FG, for stimuli presented on the contralateral (*lower right*) part of the visual field. The stimuli in rows 1 and 3 were faces and in rows 2 and 4 checkerboard oval pattern. During a run, stimulus type and location varied randomly and the subject attended either to the faces on the right (*rows 1 and 2*) or to the checkerboards on the right (*rows 3 and 4*). For each case, two single trials and the average of the six trials used in the run are displayed. (**b**). The signal and noise power and their ratio (signal to noise ratio) are computed for the six trials and are displayed for each of the cases in (**a**). (*See* Color Plate)

latency axis. We compute SP, NP and SNR as described elsewhere *(36)* and give the relevant formulae in Appendix 2. **Figure 8.2b** shows the SP, NP and SNR for the six trials in the same order as part (A) of the same figure. It is evident that using only six trials in each set is enough for a faint response pattern to be seen in the average (heavy black line in **Fig. 8.2a**) and clear strong peaks in the SNR computed using the 20 ms sliding windows across the six single trials (**Fig. 8.2b**). The high SNR values are computed from SP and NP measures that show a much smoother behavior than the raw activation curves. It is evident in **Fig. 8.2b** that the peaks in SNR values are sometimes due to increase in SP; at others, due to decrease in NP and, at yet others, due to a combination of the two. The message from **Fig. 8.2** is that the use of measures that exploit the information in single trial tomographic analysis allows reliable extraction of information from a small number *(6)* of trials. Information of similar quality is available in the average signal only when a large number (typically hundreds) of trials are averaged. The average signal of large number of trials shows peaks that cluster around the SNR peaks of regional activations, often from more than one area. These results have significant implications for experimental designs. In general, it is highly desirable to have only a few trials of a given type within a session, for example to avoid habituation, or to include many different conditions in each run. Since this is incompatible with averaging hundreds of trials, the design of most experiments becomes a choice of lesser evils. The capability of single trial tomographic analysis of each timeslice therefore allows for more powerful experimental designs, as the next example demonstrates.

The last example summarizes the results of a recent study of illusory contour perception with stimuli presented at the center of the visual field and in each of the quadrants *(37)*. Using tomographic analysis of average data from relatively few trials in each run, we were able to study in the same experiment and for each part of the visual field, the effect of attention as reflected by different task demands. The MFT solutions were used to compute activation curves mainly within the primary visual cortex (V1/V2), the lateral occipital cortex (LOC) and FG for each subject, visual field presentation, condition and stimulus type. The location of the V1/V2, LOC and FG ROIs identified for each subject were transformed into the space of Talairach and Tournoux *(38)* and finally back-projected onto the MRI of one subject for display purposes. The statistical analysis of the activation curves from seven subjects demonstrated that a different mechanism operates for the processing of illusory figure processing when the stimuli are presented in the center and periphery of the visual field *(37)*. The results are displayed in **Figure 8.3** for stimuli presented in the center (**Fig. 8.3a**) and for stimuli presented in the four quadrants (**Fig. 8.3b**) of the visual field. In

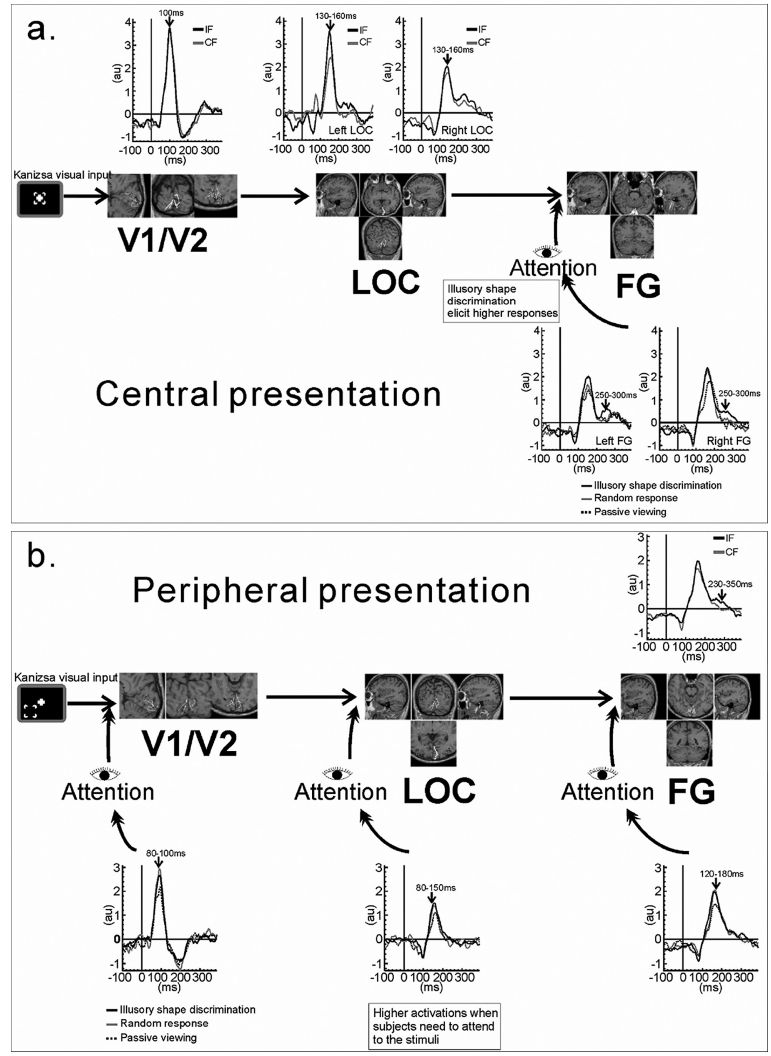

Fig. 8.3. Illusory figure processing with stimuli presented in the center (**a**) and periphery (**b**). In each case, the middle row shows cuts through each of the main areas identified by detailed MFT analysis. Dots on the MRI slices represent the center of regions of interest identified in each subject (after transformation to the space of Talairach and Tournoux *(38)*. The calcarine fissure and the V1/V2 borders (defined by an independent experiment for the subject whose MRI is used in the display) are also shown. The top row in each part shows the grand-average of the regional activations whenever a statistically significant difference between illusory contours present and absent was identified. The lower row shows similar grand-average activation curves when statistically significant differences were identified between tasks, requiring different attention levels.

parts (a) and (b) of **Fig. 8.3**, the middle row shows the location of the centers of V1/V2, LOC and FG ROIs (back-projected onto one MRI as described above) and superimposed on the nearest MRI slice used for common display. The top row (above the middle row showing the ROI locations) displays in separate

curves the grand-averages for the illusory figures (IF) and control figures (CF); the control figures have the inducers rotated so no illusory contours are perceived. The activation curves are shown only for the cases when an IF effect is present, i.e. when ANOVA has shown that the response for IF and CF was significantly different. The activation curves below the middle row show grand-averages for the three different tasks: Classification task when subjects had to indicate the presence of an (illusory) shape (illusory shape discrimination); when the subjects had to respond randomly every time an image appeared, irrespective of the presence or absence of illusory figures (random response); and when subjects simply viewed the stimuli passively (passive viewing). The activation curves are shown only for the cases when a task effect is present, i.e. when ANOVA has shown that the response for different tasks was significantly different. These results showed for the first time a distinct difference between processing when stimuli were presented to the center and periphery of the visual field. In each and every task, stimuli presented at the center produce an IF effect first in V1/V2 (~100 ms) and then in the LOC and FG (130–160 ms); this IF effect thus appears to proceed independently of attention. For center presentation, attention effects show up late, after 200 ms in the FG activation. For presentation in the periphery, no IF effects are seen early, they are seen only after 200 ms mainly in the FG. Peripheral stimuli produce early attentional effects first in V1/V2 (80–100 ms), then in LOC (80–150 ms) and finally in the FG (120–180 ms).

In summary, the results presented show that very precise information can be extracted in both the temporal and spatial domain. Very simple techniques, almost like reading the raw signal are enough for strong and superficial generators (**Fig. 8.1**). Full tomographic techniques can be used to obtain real-time information across the brain in single trials or from a small set of trials as shown in **Fig. 8.2**. The ability to extract reliable information from a small number of trials is exploited in the last example. **Figure 8.3** shows when and where illusory figure processing takes place and how task demands modulate the allocation of attention in each area. These results were obtained from a detailed MFT analysis of average MEG data from seven subjects, using only a small number of trials in each average.

5. Notes

5.1. Disadvantages

The need for shielding and use of liquid helium makes MEG an expensive technology both in terms of the cost of hardware and the operating costs. Another disadvantage of MEG is the need for the subject to stay motionless while data are collected. MEG is insensitive to radial currents; so generators close to the center

of the head (e.g. thalamus) and at the crest of gyri are close to silent sources. The patterns of activity identified with MEG are not very meaningful on their own because they lack anatomical context. The background anatomy must be provided by other methods, usually MRI, and the process of combining the background anatomy and the functional information requires considerable effort to ensure accurate coregistration between the two modalities for each subject and experiment.

5.2. Advantages

MEG is a completely non-invasive method with superior temporal resolution. With appropriate analysis methods, it can provide accurate localization of different brain regions activated simultaneously. The MEG signal depends weakly on the conductivity changes in the brain and simple models can provide accurate estimates of the magnetic field generated by a source in the brain. The insensitivity to radial sources adds to the discriminability of MEG, especially for sources in sulci.

6. Appendix 1: Lead Field Analysis

The measurements d_m (with m labeling sensors) depend on the primary current density vector $\mathbf{J}(\mathbf{r})$ via an integral over all regions with primary currents (the source space, Q),

$$\mathrm{d_m} = \int_{\mathrm{Q}} \boldsymbol{\varphi}_m(\mathbf{r}) \cdot \mathbf{J}(\mathbf{r}) \mathrm{d}\mathbf{r} \tag{8.1}$$

The vector function $\boldsymbol{\varphi}_{\mathrm{m}}(\mathrm{r})$ is known as the lead field and it describes the sensitivity profile of the m^{th} sensor. The lead field is completely determined by the geometric properties of the coils making up each sensor and the conductivity details of the biological medium. Since only vectors with non-zero overlap with at least one lead field can contribute to the signal, we can express the unknown current density vector $\mathbf{J(r)}$ as a linear sum over the lead fields, modulated by some unknown function, ω, which, in its most general form, can be a function of location *and* of the unknown $\mathbf{J}(\mathbf{r})$ itself, i.e.,

$$J(r) = \sum_{\mathrm{m}} \mathrm{A_m} \boldsymbol{\varphi}_{\mathrm{m}}(\mathrm{r}) \omega(\mathrm{r}, \mathrm{J}(\mathrm{r})) \tag{8.2}$$

The wMN solution follows from the tempting choice of setting $\omega(\mathrm{r},\mathrm{J}(\mathrm{r})) = \omega_{\mathrm{MN}}(\mathrm{r})$, i.e assuming that the function, ω, does not depend on any property of $\mathbf{J}(\mathbf{r})$,

$$J(r) = \sum_{\mathrm{m}} \mathrm{A_m} \varphi_{\mathrm{m}}(\mathrm{r}) \omega_{\mathrm{MN}}(\mathrm{r}) \tag{8.3}$$

Substituting of (8.3) in (8.1) leads to a linear system of equations. The only choice to be made is for the spatial dependence of $\omega_{MN}(r)$. This choice is usually made to smooth over biases in the sensitivity of the sensors to different parts of the source space while "projecting out" source configurations that are already present in some baseline measurement. Linearity allows such tasks to be performed at the level of signal properties as described for example in the covariance matrices of active and control conditions. Although the (w)MN choice seems natural, it can not be justified a priori. It puts an enormous load on the weight factor, ω, demanding that just its spatial dependence can recover the strength and location of generators. Effectively, the simplicity and computational advantage of the linear models is bought at the expense of using only a small amount of the information in the data.

Generalized MFT admits a power expansion of $\omega(\mathbf{r},\mathbf{J}(\mathbf{r}))$ in the modulus of the current density,

$$\mathrm{J}(\mathrm{r}) = |\mathrm{J}(\mathrm{r})|^{p+1} \sum_{\mathrm{m}} \mathrm{A_m} \varphi_{\mathrm{m}}(r) \omega_{\mathrm{p}}(\mathrm{r}) \tag{8.4}$$

Leading to a family of methods *(10, 21)*: MN, wMN and LORETTA *(19)* for $\mathrm{p} = -1$, and a version of the FOCUSS *(20)* algorithm (corrected for gauge invariance) for $\mathrm{p} = +1$. Standard MFT, as was initially selected via simulations corresponds to $\mathrm{p} = 0$ *(9, 10)*.

The way standard MFT draws on the data makes the method computationally demanding but it also confers two contrasting and highly desirable properties that are necessary for accurate and unbiased localization. First, only for standard MFT (with $\mathrm{p} = 0$) the right hand side of (8.4) depends on the modulus of the current density, just like the left hand side does, thus allowing sharp discontinuities in the current density vector with small values of the expansion coefficients. Second, standard MFT satisfies the principle of least sensitivity to both variations of the data and iterations of the non-linear norm constraints *(10)*. On the practical side, MFT allows only part of the function, ω, the a priori weight, $\omega_0(\mathbf{r})$, to be computed in advance from simulations with computer generated data *(9)* or in more general ways *(10)*. The full current density must be obtained from a highly non-linear system of equations for each snapshot of data. Specifically, the strength must be determined more explicitly from the MEG signal itself. A more detailed discussion about the theoretical basis and algorithmic implications of different choices of p can be found in *(10,21)*, and a discussion of the pitfalls of choosing values other than $\mathrm{p} = 0$ in *(32)*.

7. Appendix 2: Quantification of Signal and Noise in Timeseries

Consider the time-series, $x_i(t)$ representing either the signal of a sensor or the activation of a region of interest (ROI) for the ith single trial. For example, $x_i(t)$could be defined as$x_i(t) = \int_{ROI} J_i(r,t) \cdot \hat{u}_{ROI} d^3r$, with $J_i(r,t)$the instantaneous estimate for the current density vector at time t and trial (i) and $\hat{u}_{ROI}$ the direction of the current density vector at the maximum (modulus) of the MFT activation. A quantitative measure of the signal-to-noise ratio (SNR) can be derived from the ensemble of single trial timeseries using a conventional SNR estimator *(39)*. The spatial specificity of the MFT solutions allows such estimates to be made for relatively small segments of regional activations, and hence map their evolution across the latency axis. Around each timeslice t, we define aligned data segments $X_i(t,p) = \left[x_i(t - \frac{p-1}{2}), \ldots, x_i(t-1), x_i(t), x_i(t+1), \ldots, x_i(t + \frac{p-1}{2})\right]$ consisting of *p* samples. The noise power (NP) and signal power (SP) and SNR can then be defined using the following equations *(36, 40)*:

$$\bar{X} = \frac{\sum^N{}_{i=1} X_1(t,p)}{N}, NP = \frac{\sum^N{}_{i=1} \|\bar{X} - X_i(t,p)\|^2_{L_2}}{p(N-1)},$$

$$SP = \frac{1}{p}\|\bar{X}\|^2_{L_2} - \frac{1}{N}NP, SNR = \frac{SP}{NP}$$

For further discussion about these measures and their meaning see *(36, 41)*

References

1. Cohen, D. (1968) Magnetoencephalography: Evidence of magnetic fields produced by alpha-rhythm currents. *Science* 161, 784–786.
2. Fenwick, P. (1987) The inverse problem: A medical perspective. *Phys. Med. Biol.* 32, 5–9.
3. H.von Helmholtz (1853) ber einige Gesetze der Vertheilung elektrischer Ströme in körperlichen Leitern, mit Anwendung auf die thierisch-elektrischen Versuche. *Ann. Phys. Chem.* 89, 211, 353–233, 377.
4. Ioannides, A.A. (2001) Real Time Human Brain Function: Observations and Inferences from Single Trial Analysis of Magnetoencephalographic Signals. *Clinical EEG* 32(3), 98–111.
5. Liu, L., and Ioannides, A.A. (1996) A correlation study of averaged and single trial MEG signals: The average describes multiple histories each in a different set of single trials. *Brain Topogr.* 8, 385–396.
6. Hamalainen, M., Hari, R., Ilmoniemi, R.J., Knuutila, J., and Lounasmaa, O.V. (1993) Magnetoencephalography – Theory, Instrumentation, and Applications to Noninvasive Studies of the Working Human Brain. *Rev. Modern Phys.* 65, 413–497.
7. Darvas, F., Pantazis, D., Kucukaltun-Yildirim, E., and Leahy, R.M. (2004) Mapping human brain function with MEG and EEG: Methods and validation. *Neuroimage* 23 Suppl 1, S289–S299.
8. Hillebrand, A., Singh, K.D., Holliday, I.E., Furlong, P.L., and Barnes, G.R. (2005) A new approach to neuroimaging with magnetoencephalography. *Human Brain Map.* 25, 199–211.

9. Ioannides, A.A., Bolton, J.P.R., and Clarke, C.J.S. (1990) Continuous probabilistic solutions to the biomagnetic inverse problem. *Inv. Prob.* 6, 523–542.
10. Taylor, J.G., Ioannides, A.A., and Muller-Gartner, H.W. (1999) Mathematical analysis of lead field expansions. *IEEE Trans. Med. Imaging* 18, 151–163.
11. Ribary, U., Ioannides, A.A., Singh, K.D., Hasson, R., Bolton, J.P.R., Lado, F., Mogilner, A., and Llinas, R. (1991) Magnetic-Field Tomography of Coherent Thalamocortical 40-Hz Oscillations in Humans. *Proc. Natl. Acad. Sci. USA* 88, 11037–11041.
12. Ioannides, A.A. (2006) Magnetoencephalography as a research tool in neuroscience: State of the art. *Neuroscientist.* 12, 524–544.
13. Ioannides, A.A. (2007) Dynamic functional connectivity. *Curr. Opin. Neurobiol.* 17, 161–170.
14. Ioannides, A.A., Fenwick, P.B.C., and Liu, L.C. (2005) Widely distributed magnetoencephalography spikes related to the planning and execution of human Saccades. *J. Neurosci.* 25, 7950–7967.
15. Kominis, I.K., Kornack, T.W., Allred, J.C., and Romalis, M.V. (2003) A subfemtotesla multichannel atomic magnetometer. *Nature* 422, 596–599.
16. Bell, A.J., and Sejnowski, T.J. (1995) An information-maximization approach to blind separation and blind deconvolution. *Neural Comput.* 7, 1129–1159.
17. Sarvas, J. (1987) Basic mathematical and electromagnetic concepts of the biomagnetic inverse problem. *Phys. Med. Biol.* 32, 11–22.
18. Huang, M.X., Mosher, J.C., and Leahy, R.M. (1999) A sensor-weighted overlapping-sphere head model and exhaustive head model comparison for MEG. *Phys. Med. Biol.* 44, 423–440.
19. Pascualmarqui, R.D., Michel, C.M., and Lehmann, D. (1994) Low-Resolution Electromagnetic Tomography – A New Method for Localizing Electrical-Activity in the Brain. *Int J. Psychophysiol.* 18, 49–65.
20. Gorodnitsky, I., and Rao, B.D. (1992) Sparse signal reconstruction from limited data using FOCUSS: A re-weighted minimum norm algorithm. *IEEE Trans. Signal Process.* 45, 600–616.
21. Ioannides, A.A., and Taylor, J.G. (1999) Minimum norm, Magnetic Field Tomography and FOCUSS. Tohoku University Press, Sendai, pp. 228–231.
22. Ioannides, A.A., Singh, K.D., Hasson, R., Bauman, S.B., Rogers, R.L., Guinto, F.C., and Papanicolaou, A.C. (2007) Comparison of current dipole and magnetic field tomography analyses of cortical response to auditory stimuli. *Brain Topogr.* 6, 27–34.
23. Ioannides, A.A., Hellstrand, E., and Abrahamfuchs, K. (1993) Point and Distributed Current-Density Analysis of Interictal Epileptic Activity Recorded by Magnetoencephalography. *Physiol. Measur.* 14, 121–130.
24. Ioannides, A.A., Kostopoulos, G.K., Laskaris, N.A., Liu, L.H., Shibata, T., Schellens, M., PoghosyaN, V., and Khurshudyan, A. (2002) Timing and connectivity in the human somatosensory cortex from single trial mass electrical activity. *Human Brain Mapp.* 15, 231–246.
25. Moradi, F., Liu, L.C., Cheng, K., Waggoner, R.A., Tanaka, K., and Ioannides, A.A. (2003) Consistent and precise localization of brain activity in human primary visual cortex by MEG and fMRI. *Neuroimage.* 18, 595–609.
26. Tzelepi, A., Ioannides, A.A., and PoghosyaN, V. (2001) Early (N70m) neuromagnetic signal topography and striate and extrastriate generators following pattern onset quadrant stimulation. *Neuroimage* 13, 702–718.
27. Laskaris, N.A., Liu, L.C., and Ioannides, A.A. (2003) Single-trial variability in early visual neuromagnetic responses: an explorative study based on the regional activation contributing to the N70m peak. *Neuroimage* 20, 765–783.
28. Makeig, S., Westerfield, M., Jung, T.P., Enghoff, S., Townsend, J., Courchesne, E., and Sejnowski, T.J. (2002) Dynamic brain sources of visual evoked responses. *Science* 295, 690–694.
29. Furey, M.L., Tanskanen, T., Beauchamp, M.S., Avikainen, S., Uutela, K., Hari, R., and Haxby, J.V. (2006) Dissociation of face-selective cortical responses by attention. *Proc. Natl. Acad. Sci. U S A* 103, 1065–1070.
30. Liu, M.J., Hasson, R., and Ioannides, A.A. (1993) A transputer-based system for Magnetic Field Tomography. *Transputer Applications and Systems '93.* IOS Press, Amsterdam, pp. 1290–1297.
31. Ioannides, A.A., PoghosyaN, V., Liu, L.C., and Streit, M. (2002) Early amygdala activations in normal and schizophrenic subjects. *Soc. Neurosci. Abstr.*, p. 521.5.
32. Ioannides, A.A. (2007) MEG single-event Analysis: Networks for Normal Brain Function and Their Changes in Schizophrenia. *Complex Medical Engineering.* Springer, pp. 361–374.
33. LeDoux, J.E. (1996) *The Emotional Brain.* Simon and Schuster, New York.
34. Ioannides, A.A., PoghosyaN, V., Dammers, R., and Streit, M. (2004) Real-time neural activity and connectivity in healthy individuals and schizophrenia patients. *Neuroimage* 23, 473–482.

35. Luo, Q., Holroyd, T., Jones, M., Hendler, T., and Blair, J. (2007) Neural dynamics for facial threat processing as revealed by gamma band synchronization using MEG. *Neuroimage* 34, 839–847.
36. Laskaris, N.A., and Ioannides, A.E. (2001) Exploratory data analysis of evoked response single trials based on minimal spanning tree. *Clin. Neurophysiol.* 112, 698–712.
37. Abu Bakar, A., Liu, L.C., Conci, M., Elliot, M.A., and Ioannides, A.A. (2008, In press) Visual Field and Task Influence Illusory Figure Responses. *Human Brain Mapping.*
38. Talairach, J., and Tournoux, P. (1988) *Co-planar stereotaxic atlas of the human brain.* G. Thieme, Stuttgart ; New York.
39. Raz, J., Turetsky, B., and Fein, G. (1988) Confidence-Intervals for the Signal-To-Noise Ratio When A Signal Embedded in Noise Is Observed Over Repeated Trials. *Ieee Transactions on Biomedical Engineering* 35, 646–649.
40. Laskaris, N., Fotopoulos, S., Papathanasopoulos, P., and Bezerianos, A. (1997) Robust moving averages, with Hopfield neural network implementation, for monitoring evoked potential signals. *Evoked Potentials-Electroencephalography and Clinical Neurophysiology* 104, 151–156.
41. Liu, L.C., Fenwick, P.B.C., Laskaris, N.A., Schellens, M., PoghosyaN, V., Shibata, T., and Ioannides, A.A. (2003) The human primary somatosensory cortex response contains components related to stimulus frequency and perception in a frequency discrimination task. *Neuroscience* 121, 141–154.